Testing several methods for the fusion of the two HelioClim-1 and-3 data sets of daily downwelling solar radiation at surface-Application to the creation of a new consistent 1985-2016 data set

Benoît Gschwind, Lucien Wald

Technical Note – 2019-01-05

Benoît Gschwind, Lucien Wald

MINES ParisTech, PSL University, O.I.E. - Center for Observation, Impacts, Energy, Sophia Antipolis, France

Testing several methods for the fusion of the two HelioClim-1 and -3 data sets of daily downwelling solar radiation at surface – Application to the creation of a new consistent 1985-2016 data set

Abstract: The HelioClim-1 and -3 data sets provide satellite-derived estimates of the daily downwelling solar radiation at the surface at different spatial and temporal resolutions and different periods with an overlap of 23 months in 2004-2005. Eight methods are tested for fusing HelioClim-1 and -3 to create an enhanced version HC1e of HelioClim-1 having a better accuracy. The methods apply to the irradiation as well as to the clearness index *KT* and include adjustment by addition, ratioing, affine transforms, and quantile mapping. The comparison with measurements performed at nine meteorological stations for the period 1985-2003 reveals that the affine transform and quantile mapping of *KT* yield the best results. As an application, a new data set, called SSRD-H3E, has been created by the concatenation of HC1e and HelioClim-3 using the quantile mapping of *KT* technique. It offers daily mean of irradiance at the surface and at the top-of-the-atmosphere over 1985-2016 with a spatial resolution of 0.25°. When compared to the measurements at the nine stations from 1985 to 2016, the standard deviation of errors is less than 29 W m^{-2} (250 J cm^{-2} for daily irradiation); the correlation coefficient is always greater than 0.92.

1. Introduction

The downwelling solar radiation incident on the surface of the Earth is known to be an essential variable in many domains. The solar irradiation is the density of energy received from the Sun on a horizontal surface at ground level and per unit surface, while the irradiance is the density of power. Other terms may be found in literature, such as solar exposure or solar flux, surface solar irradiation, downwelling shortwave irradiation, downwelling lar irradiation at the surface, or global surface irradiation. "Surface Solar Radiation Downward" (SSRD) is often used in reanalyses and is adopted in the following; it may refer either to irradiation or irradiance depending on the context.

Accurate assessments of the SSRD can be made from satellite images, see e.g. Amillo et al. (2014), Chen et al. (2014), Karlsson et al. (2017), Müller et al. (2015), or Pfeifroth et al. (2017). The series of geostationary Meteosat satellites offer synoptic views of Europe, Africa and the Atlantic Ocean since 1983 with a spatial resolution of approximately 5 km at nadir and a temporal frequency of 30 min for the first generation and 3 km and 15 min for the second one. Several data sets of SSRD have been constructed from these images, such as the Surface Radiation Data Set – Heliosat (SARAH-2) (Pfeifroth et al., 2017) or the Copernicus Atmosphere Monitoring Service (CAMS) Radiation Service (Qu et al., 2017).

Of particular interest here are the HelioClim-1 and -3 data sets of SSRD constructed from Meteosat imagery. The HelioClim Project is an ambitious initiative of MINES ParisTech launched in 1997 to increase the knowledge about SSRD and to offer data over a large geographical area and over a long period of time, to a wide audience (Blanc et al., 2017). The project comprises the creation and management of several SSRD data sets, called HelioClim data sets and abbreviated hereafter as HC. Though they cover the same geographical area, the HC1 and HC3 data sets have different spatial and temporal resolutions, different accuracies, and different temporal coverages with an overlap of 23 months from February 2004 to December 2005. HC1 offers daily irradiation with a spatial resolution of approximately 30 km for the period 1985-2005. Given SEVIRI having 3 km of resolution at nadir, HC3 contains 15 min SSRD with a spatial resolution of approximately 5 km for the period from February 2004 onwards.

Benefiting from the fact that HC1 and HC3 share an overlap period, we have undertaken in this technical note to demonstrate the better accuracy of HC3 over HC1 and then improve the accuracy of HC1 using HC3 data set and a data fusion method. The main objective of this note is to study the merits and drawbacks of eight methods to perform this fusion of HC1 and HC3. Data fusion has been defined by the European Association of Remote Sensing Laboratories (EARSeL) as a formal framework in which are expressed means and tools for the alliance of data originating from different sources. It aims at obtaining information of greater quality; the exact definition of 'greater quality' will depend upon the application (Wald, 1999).

Given a specific location, the fusion process adopted here locally adjusts the HC1 time series of daily SSRD onto coincident HC3 daily SSRD for the common period 2004-2005 to benefit from the better accuracy of HC3. The adjustment is performed at each pixel and is applied to the whole data set from 1985 to 2005. In other words, it creates an enhanced HC1 data set, abbreviated as HC1e, which, hopefully, is more accurate than the original HC1. The greater quality may be proven by a comparison with qualified ground measurements of the daily SSRD. The possible improvement in bias and other statistical indicators are assessed by comparing the performance of the original HC1 against these ground measurements on the one hand and those of the HC1e against these same measurements on the other.

The large use of the HC1 data by many researchers in various domains as reported by Lefèvre et al. (2014) supports this work and justifies providing some guidance to users of the HC1 data set so that they can implement themselves a fusion method.

As an application, a new data set, called SSRD-H3E, has been created by the concatenation of HC1e and HelioClim-3 using the quantile mapping of KT technique. This data set of consistent 1985-2016 time series of daily SSRD over Europe and Africa is publicly available and is called SSRD-H3E. It has been built with a spatial resolution of 0.25°. Its presentation and validation are another goal of this note.

Section 2 details the HC1 and HC3 data sets and presents the nine stations in Europe and Africa that are used for validation only. Section 3 presents the results of the comparison between the ground measurements and HC1 on the one hand, and HC3 on the other, for the 23 common months in 2004-2005. Such a comparison has not been published up to now to the best of the knowledge of the authors. It shows the greater accuracy achieved by HC3 thus highlighting the potential of a fusion.

The eight fusion methods are described in Section 4. In Section 5, they are applied to HC1 and validated at the 9 stations for the period 1985 to 2003 prior to the calibration period 2004-2005. Conclusions are drawn on the merits and drawbacks of each method.

Section 6 describes the SSRD-H3E data set and its validation for the same stations and the whole period 1985-2016 as well as for each year in this period, thus assessing the reliability of the performance with time. Section 7 concludes the note.

An annex provides a few lines of the Python code for implementing an adjustment based on quantile mapping.

2. Data sets

2.1. The HC1 and HC3 data sets

The HC1 data set has been constructed with images acquired between 1985 and 2005 by broadband imagers aboard the various Meteosat First Generation satellites. At the start of the HelioClim project in 1997, the large amount of data to be processed, the storage capacity, and the cost of the Meteosat images from the Eumetsat agency were obstacles to the production of a data set (Blanc et al., 2007). A data set of Meteosat images in reduced spatial and temporal resolutions has been purchased to overcome these obstacles. This data set was created for the International Satellite Cloud Climatology Project (ISCCP) and is called ISCCP-B2 (Schiffer, Rossow, 1985). These images can be considered as having a spatial resolution of 30 km at nadir in a first approximation (Blanc et al., 2007). A great deal of effort was made to ensure the radiometric consistency of all these ISCCP-B2 images, so that the quality of the estimated SSRD is the same throughout the whole period at a given pixel (see details in Blanc et al., 2007). Because of the reduced temporal resolution, HC1 offers only daily SSRD.

The time sampling of the ISCCP-B2 images every 3 h induces limitations in the description of the daily mean of SSRD in HC1. A discrepancy between HC1 and HC3 is created by this effect, whose magnitude depends on the temporal variability of the SSRD as discussed by e.g. England and Hunt (1984). Blanc et al. (2007) have studied the effect of the low number of ISCCP-B2 images usable per day on the difference between HC1 and HC3 for a given pixel; this number decreases as the latitude increases, and so does the quality of the HC1 retrieval as a whole. When investigating ocean pixels only in order to avoid effects of orographic origin, these authors found that this difference has a tendency to increase with the absolute value of the latitude, i.e. with the decreasing number of available ISCCP-B2 images, and that the difference decreases as the clearness index increases: i.e. for a given range of latitude, the error is smaller in case of clear skies. However, Blanc et al. (2007) underlined that outside the ocean pixels, the effect of the limited number of satellite observations within a day cannot be easily predicted. This shows in Section 3 where HC1 and HC3 are compared against ground measurements.

The HC3 data set is being constructed from images acquired by the multispectral imagers of SEVIRI aboard the operational series of Meteosat Second Generation satellites since their operational inception in February 2004. Contrary to the Meteosat First Generation images used for HC1, Eumetsat is embedding elements for the radiometric calibration in each SEVIRI image, ensuring the radiometric consistency of images. Once the images converted in radiances, and to improve the consistency between HC1 and HC3, the radiances of the two narrow visible bands of the SEVIRI at 600 nm and at 800 nm are combined to produce broadband radiances that are almost identical to those observed in the broadband channel of the imager aboard the Meteosat First Generation satellites (Cros et al., 2006). As those synthetic broadband radiances are similar to those used for HC1, the same method is applied to retrieve the SSRD, namely the Heliosat-2 method combined with the ESRA clear-sky model (see details in Lefèvre et al., 2007). A clear-sky model is a model predicting the SSRD in cloud-free conditions. The volume of data to be processed, the storage capacity, and the cost were not any longer obstacles

in 2004, thus HC3 is built with the full temporal and spatial resolutions of the images, respectively 4 images per hour and 3 km at nadir.

The HC1 and HC3 data sets are live collection of data and are corrected a posteriori as flaws or drawbacks are discovered, yielding several versions. HC1v4 and HC3v5 are the most recent versions, the latter being obtained by the use of the Copernicus McClear clear-sky model (Lefèvre et al., 2013) following the method of Qu et al. (2014). The HC1 and HC3 data sets have been the subject of several comparisons against measurements of SSRD made at land-based sites or oceanic moorings, see references in Lefèvre et al. (2014) for HC1 and see e.g. Trolliet et al. (2018) and its references for HC3.

For this work, the HC1, HC3 and the top-of-the-atmosphere time series of daily irradiation, respectively G_{hc1}, G_{hc3} and *G0*, have been downloaded from the SoDa Service (Gschwind et al., 2006) (http://www.soda-pro.com). The clearness indices KT_{hc1} and KT_{hc3} are respectively defined as the ratios $G_{hc1}/G0$, and $G_{hc3}/G0$. The clearness index is an indicator of the atmospheric transparency. It depends on several factors such as cloud presence and properties, content in water vapor or aerosol properties, and is a means to characterize the gross influence of clouds as the latter are the most influencing factor on the extinction of solar radiation by the atmosphere. It is typically close to 0.8 in cloud-free conditions, and close to 0.1 in overcast conditions with optically thick clouds.

2.2. Description of the stations and their measurements

Time series of daily irradiation G_{wrdc} were downloaded from the web site (http://wrdc.mgo.rssi.ru) of the World Radiation Data Center (WRDC), a laboratory of the Voeikov Main Geophysical Observatory in Saint Petersburg, Russia, under the control of the World Meteorological Organization (WMO). G_{wrdc} is given in J cm^{-2} as is usual in meteorology. If necessary, the daily mean of irradiance E_{wrdc} is obtained by converting G_{wrdc} in J m^{-2} and dividing the result by the number of seconds in 24 h:

$$E_{wrdc} = G_{wrdc} * 10000 / (24 \times 3600) = G_{wrdc} * 0.11574, \text{ in W m}^{-2}. \quad (1)$$

The values of G_{wrdc} were kept only when the quality flags set by WRDC were equal to 0 (“good value”). Otherwise, the corresponding day was declared as having invalid measurements. An additional visual screening was performed by the authors, looking for possible anomalies and rejecting very low values. This screening took into account the WMO guide on measurements of solar radiation (WMO, 2012) that says that the relative uncertainty (95 % probability) for “good quality” of measurements is 5 % if G_{wrdc} > 800 J cm^{-2}; otherwise the uncertainty is set to 40 J cm^{-2}.

Nine stations (Table 1) were used in this work spanning the period 1985-2016. Each station offers enough data for most of the years, i.e. *i)* more than 85 % of the days within a year bear valid daily SSRD, *ii)* no more than 5 days are missing within a month and *iii)* possible gaps cover less than 5 consecutive days. The constraints were somehow relaxed at the station Toravere, and to a lesser extent at Valentia, where the sun is very low above horizon in December and January yielding possible very low G_{wrdc} that may fall below the uncertainty. The constraint on the number of missing days was relaxed at the station Toravere (up to 15 days), and to a lesser extent at Valentia (up to 10 days), where the sun is very low above horizon in December and January yielding possible very low G_{wrdc} that may fall below the uncertainty. Using several periods is a means to assess the reliability of the performances with time. The filtered data set is available at (ftp://ftp.oie-lab.net/pub/hc1_hc3_article/ground_measurements_gschwind_wald.zip).

Table 1. List of stations, their geographical coordinates and climate

Station	Country	Latitude[1]	Longitude[1]	Altitude asl (m)	Climate (from Peel et al., 2007)
Toravere	Estonia	58.250	26.467	70	Dfb: Cold climate without dry season and warm summer
Valentia Obs	Ireland	51.933	-10.250	9	Cfb: Temperate climate without dry season and warm summer
Wien Hohe Warte	Austria	48.250	16.367	203	Dfb
Auxerre	France	47.800	3.550	207	Cfb
Payerne	Switzerland	46.815	6.944	491	Dfb
Carpentras	France	44.083	5.059	100	Csb: Temperate climate with dry and warm summer
Nice	France	43.650	7.200	4	Csb
El Arish	Egypt	31.083	33.750	31	BWh
Maputo	Mozambique	-25.967	32.600	70	Aw: Tropical savannah

[1] Coordinates follow the ISO standard, where positive latitude, respectively longitude, means Northern hemisphere and East of longitude 0°.

Figures 1, 2 and 3 provide the number of coincident valid daily irradiations per valid year between the WRDC measurements and HC1 and SSRD-H3E estimates, as well as the corresponding means of G_{wrdc} and KT_{wrdc} for each year at each station. Payerne, and Nice are the stations offering the greatest number of valid years (31); El Arish (13) and Valentia (20) are those offering the least (Fig. 1). As a whole, El Arish exhibits the greatest means of G_{wrdc} (Fig. 2) because it experiences many cloud-free days (KT_{wrdc}>0.60 in Fig. 3). Then comes Maputo which is close to the Equator and thus it experiences large extraterrestrial daily irradiations *G0*. Carpentras and Nice are located in the Provence in France and experience a large number of cloud-free days with means of KT_{wrdc} close to 0.55 (Fig. 3).

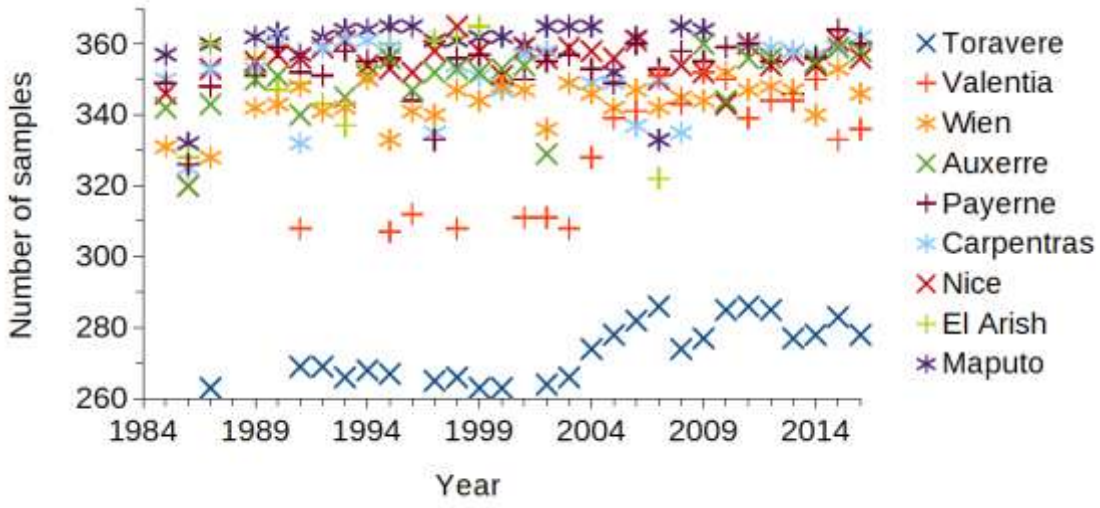

Figure 1. Number of coincident valid daily irradiations per year between the WRDC measurements and HC1 estimates from 1985 to 2016, or the SSRD-H3E estimates from 2004 to 2016 at each station

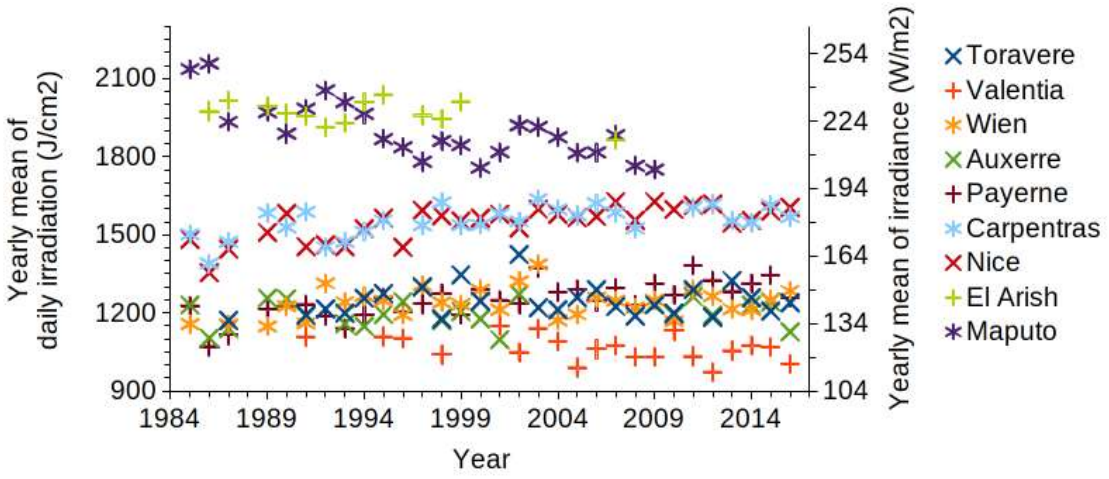

Figure 2. Yearly means of daily irradiation G_{wrdc} from WRDC at each station in the period 1985-2016. Yearly means of irradiance on the right axis

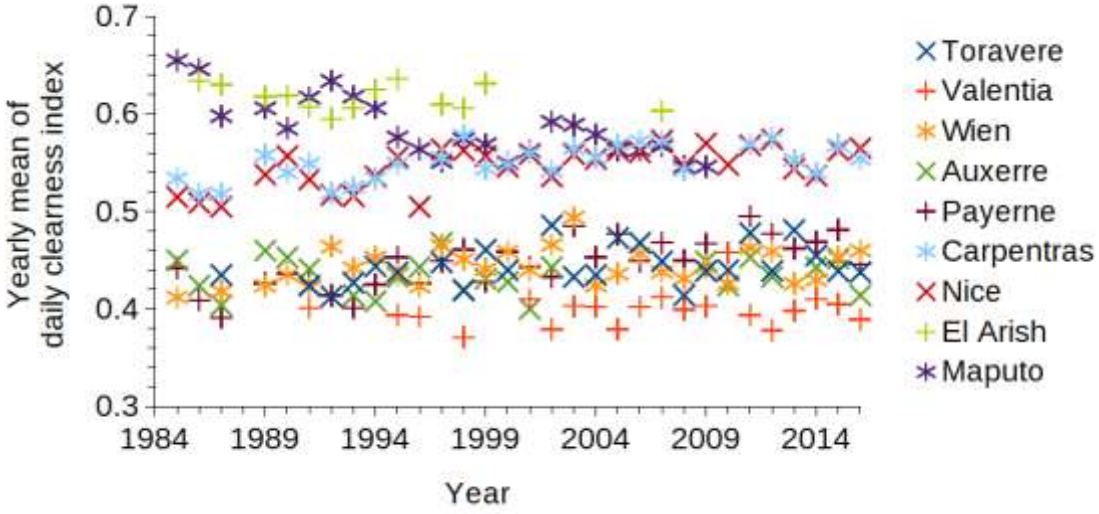

Figure 3. Yearly means of daily clearness index KT_{wrdc} from WRDC at each station in the period 1985-2016

These measurements were not used in the fusion process and were solely used for *i)* the comparison of the accuracies of HC1 and HC3 in the period 2004-2005, *ii)* the validation the 8 HC1e data sets resulting from the fusion methods, and *iii)* the validation of the new data set SSRD-H3E. The validations were performed by comparing the time series from a given data set: HC1, HC3, HC1e, SSRD-H3E, against coincident measurements at stations. The differences were summarized by the bias (mean of the differences), their standard deviation, the correlation coefficient and the slope of the fitting line between measurements and estimates. These four indicators are those dealt with in this technical note though additional indicators and graphs were computed and drawn to provide an in-depth view of the differences. The bias denotes the systematic error. A very large correlation coefficient combined with a slope close to 1 and a low standard deviation ensures that the variability of the measurements is well reproduced by the satellite-derived data set.

In the comparison process against ground-based measurements, the two time series have different spatial supports of information: measurements are for a single point in space, whereas the estimated irradiances are for

the area of a pixel (3 km for HC3v5 and 30 km for HC1 at nadir) or a grid cell (0.25° for SSRD-H3E). This approach is that used in many comparisons of satellite-derived quantities or meterological reanalyses. It means implicitly that the SSRD at coarse scale and at point-like scale can be compared and further that the SSRD is homogeneous at the coarse scale, i.e. does not offer any noticeable variation in space. This may reveal wrong depending on the site as cloud properties, including presence and optical depth, may vary within the pixel or grid cell. Such issues have been discussed long ago with respect to solar radiation, see e.g. Hakuba et al. (2013), Pinker and Laszlo (1991), or Zelenka et al. (1999). The magnitude of the effect due to the sole change in spatial support would depend on the actual underlying spatial variability of the SSRD. The lower this variability, the lower the magnitude of the effect. Most of the selected sites are in areas fairly homogeneous in terms of climate, orography and land cover and we may expect the effect of the differences in spatial support of information to be limited, because we are dealing with daily means. Using monthly averages is a means to further reduce the errors (Zhao et al., 2015). The Nice station is on the coast and may be affected though it does not clearly show on the performances when comparing with SSRD-H3E in Section 6. Zelenka et al. (1999) studied the differences between the readings of ground-based pyranometers at different timescales and different distances in homogeneous areas. They found a standard deviation of 10–15% within 10 km relative to the hourly mean of SSI. Although it is difficult to predict because spatial variability is not a random variable and depends on each location and time because of the spatial and temporal properties of the cloudiness, we can expect an error of several per cent relative to the daily mean of SSRD. It should be noted that this error due to the mismatch in spatial support may not necessarily add to the error due to the sole modelling and that both errors can counter-balance, yielding more accurate results than expected.

3. Comparison of the accuracies of HC1 and HC3 in the period 2004-2005

Prior to the presentation of the fusion methods, this section presents the results of the comparison between the ground measurements and HC1 on the one hand, and the ground measurements and HC3 on the other, for the 23 common months in 2004-2005. To the best of the knowledge of the authors, such a comparison has not been published up to now and it is believed it was necessary to show the potential of a fusion of HC1 with the more accurate HC3.

Table 2 reports the bias, standard deviation of errors, correlation coefficient and slope of the fitting line for both HC1 and HC3 at each station.

Table 2. Comparison of the accuracies of HC1 and HC3 estimations at each station in the period 2004-2005

Station	Mean daily irradiation (J cm^{-2})	Bias (J cm^{-2})		Standard deviation of errors (J cm^{-2})		Correlation coefficient		Slope (unitless)	
		HC1	HC3	HC1	HC3	HC1	HC3	HC1	HC3
Toravere	1267	-205	-24	265	157	0.941	0.979	1.051	1.003
Valentia	1109	-22	38	296	162	0.927	0.979	1.081	1.051
Wien	1212	-285	-10	335	143	0.902	0.983	0.937	1.020
Auxerre[1]									
Payerne	1289	-314	-28	330	166	0.922	0.982	0.888	1.041
Carpentras	1630	-162	28	264	109	0.954	0.993	0.978	0.967
Nice	1613	-169	50	236	114	0.960	0.991	0.920	1.000
El Arish	1838	101	46	237	153	0.951	0.974	1.180	1.067
Maputo	1816	-59	-15	236	134	0.935	0.978	1.035	0.984

[1] Not enough data from the WRDC for this period

The bias is negative for HC1 and ranges from -314 (-24 % in relative value) to -22 J cm^{-2} (2 %) with the exception of El Arish where the bias is positive (101 J cm^{-2}, 5 %). The variation of the bias for HC3 is smaller as

it ranges from -28 (-2 % in relative value) to 50 J cm^{-2} (3 %). The standard deviation of the errors ranges from 236 (13 %) to 335 J cm^{-2} (28 %) for HC1. It is much less for HC3 than for HC1 at all stations as it ranges from 109 (7 %) to 166 J cm^{-2} (13 %). The correlation coefficient is very large for HC1 but it is even greater for HC3. The slope of the fitting line for HC3 is similar to, or closer to 1 than that for HC1.

These figures demonstrate that HC3 is more accurate than HC1. Hence, this establishes the potential of an improvement of the accuracy of HC1 by a data fusion method.

4. Description of the eight fusion methods

The information entering a fusion process should present several properties (Pau, 1988). The data to be fused must be aligned, i.e. they must be represented within a common geographical time system. This is solved by using functions converting the image coordinates into latitude and longitude and using this canonical representation for geographical reference, and by using daily irradiation for both data sets.

Several methods were tested for the fusion. A brief review of other methods can be found in Polo et al. (2016). The principle of the fusion is as follows. Given a method *f*, its parameters are established by comparing G_{hc1} and G_{hc3}, or KT_{hc1} and KT_{hc3}, for the common period February 2004 to December 2005 (23 months). Then, *f* is applied to G_{hc1} to yield the enhanced data set G_{hce}. If *f* applies to KT_{hc1}, then it yields KT_{hce} which after multiplication by *G0* yields G_{hce}.

4.1 Adjustment of means or medians (P50I and P50K)

One of the simplest methods consists of computing the means, or the medians, of G_{hc1} and G_{hc3} and then adding the difference of means or medians to G_{hc1} to yield G_{hce}, here denoted as G_{hcP50I} and G_{hcP50K}. For the sake of simplicity, only the version with the median is presented as both versions give similar performances:

$$G_{hcP50I} = G_{hc1} + (median(G_{hc3}) - median(G_{hc1})), \quad (2)$$

$$G_{hcP50K} = G0\ [KT_{hc1} + (median(KT_{hc3}) - median(KT_{hc1}))]. \quad (3)$$

It can be mathematically demonstrated that the standard deviation of errors, the correlation coefficient and the slope of the fitting line are the same for G_{hc1} and G_{hcP50I}. No improvement can be expected for these indicators.

4.2 Ratioing methods (RatioI and RatioK)

The third and fourth tested methods compute a ratio of the means of G_{hc1} and G_{hc3}, or KT_{hc1} and KT_{hc3}, and then multiply G_{hc1}, or KT_{hc1}, by this ratio:

$$G_{hcRatioI} = G_{hc1}\ (mean(G_{hc3}) / mean(G_{hc1})), \quad (4)$$

$$G_{hcRatioK} = G0\ [KT_{hc1}\ (mean(KT_{hc3}) / mean(KT_{hc1}))]. \quad (5)$$

It can be mathematically demonstrated that G_{hc1} and $G_{hcRatioI}$ have the same correlation coefficient. No improvement can be expected for this indicator.

4.3 Affine functions (AffI and AffK)

An affine function $f = a\ G_{hc1} + b$ is adjusted onto G_{hc3}. It is then applied to G_{hc1} to yield G_{hcAffI}. Same approach for *KT* to yield G_{hcAffK}. The parameters *a* and *b* may be computed by a least square fitting or axis of inertia. For the least-square fitting, the parameters *a* and *b* are given by:

$$a^2 = cov(G_{hc3}, G_{hc1}) / var(G_{hc1}), \quad (6)$$

$$b = mean(G_{hc3}) - a\ mean(G_{hc1}), \quad (7)$$

where *cov* denotes the covariance, and *var* the variance.

The parameters *a* and *b* for the first axis of inertia are given by:

$$a = [[var(G_{hc3})-var(G_{hc1})] + \sqrt{[(var(G_{hc3})-var(G_{hc1}))^2 + 4\ cov(G_{hc3}, G_{hc1})]}] / cov(G_{hc3}, G_{hc1}), \quad (8)$$

$b = \text{mean}(G_{hc3}) - a\ \text{mean}(G_{hc1})$. (9)

The results are fairly similar between both adjustment techniques. Hereafter the results for the first axis of inertia are presented. It can be mathematically demonstrated that G_{hc1} and G_{hcAffI} have the same correlation coefficient. No improvement can be expected for this indicator.

4.4 Quantile mapping (QMI and QMK)

The method of 'quantile mapping' consists of adjusting the cumulative distribution function of G_{hc1} onto that of G_{hc3} for the calibration period, thus yielding an abacus that is used to convert the G_{hc1} data set into G_{hcQMI}, or G_{hcQMK} if the quantile mapping is applied to KT_{hc1} and KT_{hc3}. A pseudo-code in Python is given in Annex A.

5. Quality of each fusion method

If the fusion is efficient, the following improvements in the indicators characterizing the quality of the fusion are expected:

- the absolute value of the bias should decrease for HC1e compared to HC1,
- the standard deviation should decrease for HC1e compared to HC1,
- the correlation coefficient should increase for HC1e compared to HC1,
- the slope *s* of the fitting line should be closer to 1 for HC1e than for HC1. In other words, the absolute value of the difference between the slope and 1: $\|s-1\|$, should be closer to 0 for HC1e than for HC1. This is the approach adopted here for a better visual analysis of the possible benefit of the fusion.

In the following, each fusion method is calibrated using the 23 common months of HC1 and HC3, and then applied to HC1 and validated at the 9 stations for the period 1985 to 2003 prior to the calibration period 2004-2005. Results are analyzed with respect to the expectations listed above.

5.1 Results of the tested fusion methods

Figure 4 exhibits the absolute value of the bias at each station for the original HC1 and the results each fusion method. A benefit is obtained by a fusion method if the absolute value of the corresponding bias is less than that for HC1, in red. The bias for HC1 is less than 100 J cm^{-2} at six stations in absolute value. It amounts to 240 J cm^{-2} at Wien (20 % of the yearly mean of the daily irradiation), 186 J cm^{-2} at Auxerre (16 %) and 240 J cm^{-2} at Payerne (14 %). Any of the fusion methods brings an improvement at Wien, Auxerre, Payerne, and Maputo. On the contrary, the bias is degraded at Valentia, Carpentras, Nice and El Arish whatever the method. Surprisingly, the *P50I* and *P50K* methods do not improve the bias at each station. The good adjustment obtained for the calibration period is not always appropriate to this former period. On the contrary, the bias is significantly increased by *P50I* at Carpentras and Nice. *RatioK* performs as one of the worst methods while *RatioI*, *AffI*, *AffK*, *QMI*, and *QMK* provide the best results among the eight methods as a whole.

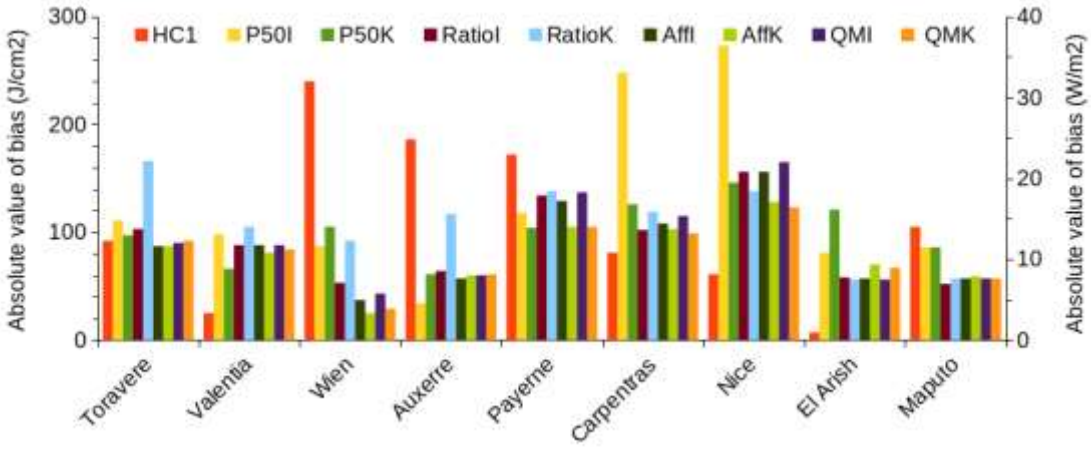

Figure 4. Absolute value of the bias at each station for the original HC1 and the results of the each fusion method in the period 1985-2003. In irradiance on right axis.

Figure 5 exhibits the standard deviation of errors at each station for the original HC1 and the results from each fusion method. A benefit is obtained by a fusion method if the corresponding standard deviation is less than that for HC1. The standard deviation mostly ranges between 220 and 270 J cm^{-2} for G_{hc1}. As written before, *P50I* has the same standard deviation than HC1: there is no benefit. *P50K* offers a status quo as a whole. *RatioI* and *RatioK* degrade the performance as the standard deviations are greater than those for HC1. Exceptions are found at El Arish and Maputo where a slight improvement and a status quo, respectively, are observed. *AffI* and *QMI* behave similarly. Except at El Arish, they exhibit a status quo or a degradation of performance. *AffK* and *QMK* behave similarly and tend to exhibit a standard deviation less than that of HC1.

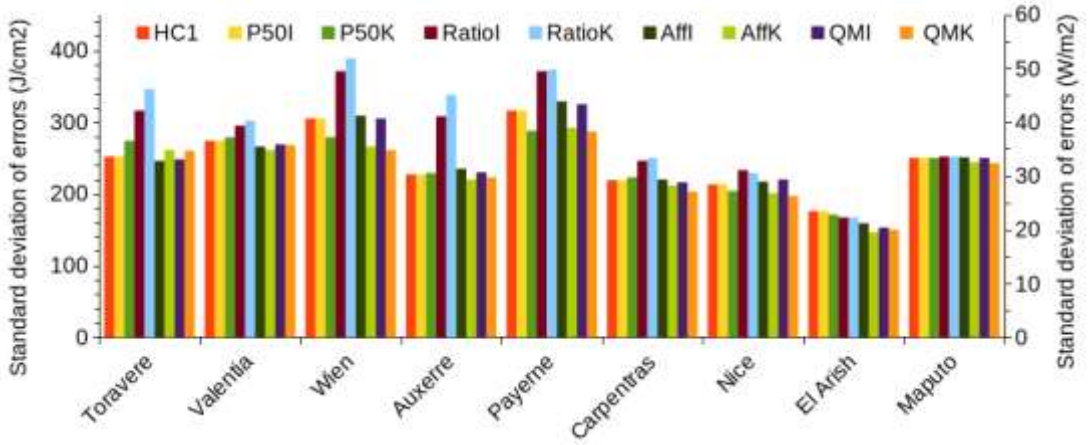

Figure 5. Standard deviation of errors at each station for the original HC1 and the results of the each fusion method in the period 1985-2003. In irradiance on right axis.

Figure 6 exhibits the correlation coefficient at each station for the original HC1 and the results from each fusion method. A benefit is obtained by a fusion method if the corresponding correlation coefficient is greater than that for HC1. The correlation coefficient for G_{hc1} is large and greater than 0.92 in all cases. As written before, *P50I*, *RatioI*, and *AffI* have the same correlation coefficient than HC1: there is no benefit. Actually, *RatioK* exhibits also the same correlation coefficients as HC1. *QMI* tends to slightly increase the correlation. *P50K*, *AffK* and *QMK* behave similarly and offer correlation coefficients greater than those of HC1. Exceptions are at Valentia where there is a status quo, and at Toravere where there is a status quo for *P50K* and a slight degradation for *AffK* and *QMK*.

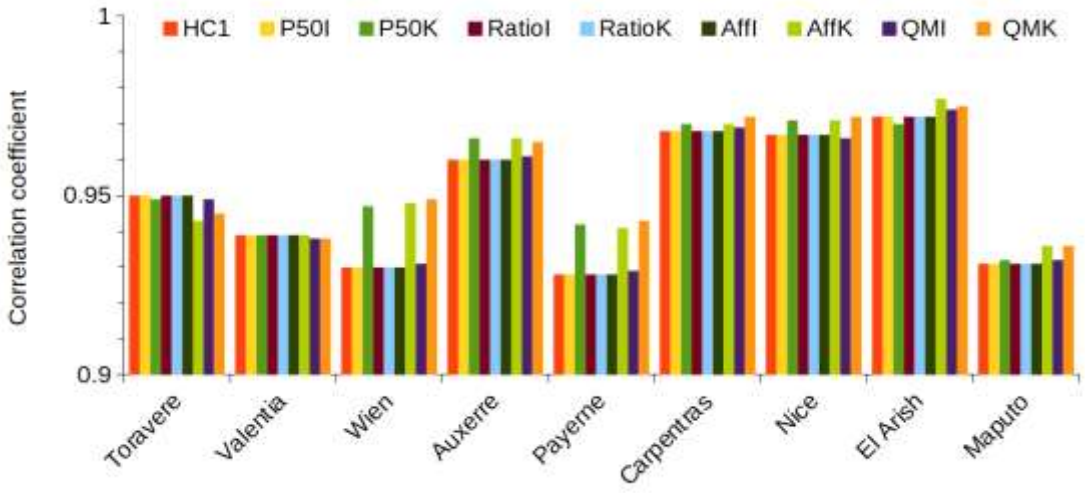

Figure 6. Correlation coefficient at each station for the original HC1 and the results of the each fusion method in the period 1985-2003

Figure 7 exhibits the absolute difference between the slope of the fitting line and 1 at each station for the original HC1 and the results from each fusion method. A benefit is obtained by a fusion method if this indicator is closer to 0 than that for HC1. The slope for G_{hc1} is close to 1.00±0.11 at all stations. As written before, *P50I* has the same slope than HC1: there is no benefit. The results for *P50K* are highly variable and offer either noticeable improvements (Wien, Payerne, Nice, El Arish) or noticeable degradation (Toravere, Valentia, Auxerre, Carpentras). *RatioI* and *RatioK* degrade the performance at all stations, except at El Arish and Maputo where an improvement is observed. *AffI*, *AffK*, *QMI*, and *QMK* behave fairly: the slope is improved at all sites, except at Auxerre and Maputo where degradation is observed.

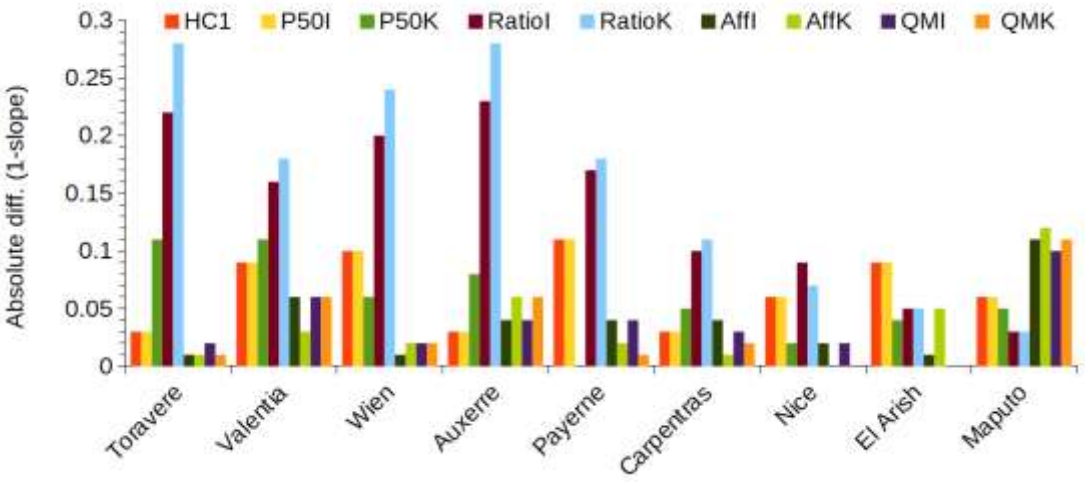

Figure 7. Absolute difference between the slope of the fitting line and 1, at each station for the original HC1 and the results from each fusion method in the period 1985-2003. The closer the difference to 0, the better.

As a summary, the benefit of adjustment of the irradiance *P50I* is limited to the bias as the other statistical indicators are left unchanged. The adjustment of the clearness index *P50K* brings more improvement compared to *P50I* regarding also the other indicators. One may conclude that the fusion by adjustment of medians may bring a benefit in some cases but an improvement is not obtained at each station and each period. *RatioI* and *RatioK* offer both improvement and degradation for the bias depending on the station. They tend to degrade the performances of HC1 for the three other indicators or to offer a status quo. *AffI* and *QMI* on the one hand, and

AffK and *QMK* on the other tend to behave similarly. While *AffI* and *QMI* show a tendency to degrade the standard deviation or to offer a status quo, *AffK* and *QMK* tend to improve it. The four methods tend to improve the two other indicators or offer a status quo.

5.2 Discussion on the performance of the tested fusion methods

This assessment of performance shows that the results are not satisfactory for the simplest methods: *P50I*, *P50K*, *RatioI* and *RatioK*. There is no benefit brought by them, and even more one may observe degradation in performance. The other methods: *AffI*, *AffK*, *QMI* and *QMK* usually offer improvement to all indicators, though degradation may be observed for the bias. We have seen no clear picture of the relationship between the performances of a method and the station (climate, latitude, mean value, performance of HC1).

As a conclusion, one notes that an efficient fusion is hard to obtain for all periods and at all stations simultaneously. Reducing the bias is the greatest difficulty. Analysis of graphs (not shown) shows that the bias is more and more reduced from 1985 to 2004 as a whole as the year approaches the calibration period but it may still be degraded for the early years. A solution should be devised for that but it would not be simple given the short overlap between HC1 and HC3.

It was found that the methods applying to the clearness index behave better than those applying to the irradiation. *QMK* and *AffK* perform similarly for the bias and the standard deviation, *QMK* exhibits slightly greater correlation coefficients and *AffK* offers better results for slope. Hence, one may conclude that both methods are equivalent with respect to the studied indicators.

The affine model deals with mean, covariance and variances, while quantile mapping applies to the cumulative distribution functions. The latter could be a disadvantage since the original cumulative distribution function of HC1 at a pixel for the whole period 1985-2005 is forced to be close to that of HC3 for the period 2004-2005. However, the tests shown here demonstrate that there is no major drawback with this approach. Further tests applied to the cumulative distribution functions and quantiles (not shown) show that *QMK* tends to slightly better represent the cumulative distribution functions than the other methods. This is the reason why the *QMK* method was used to create the new SSRD-H3E which is described in the following section.

6. The new SSRD-H3E

The new SSRD-H3E data set is an attempt to offer consistent time series of daily mean of irradiance over the period 1985-2016 and after as updates of HC3 are available. This section describes this data set and its validation for the same stations and periods as above.

6.1 Construction of the SSRD-H3E data set and its access

To begin with, the HC3 data sets were aligned on the same temporal step, same geographical area, same spatial resolution and same grid cells of HC1 dataset. HC3 were computed on a latitude-longitude grid with a cell of 0.05° in size and summarized to daily irradiation. Then, a truncated and apodized sinus cardinal filters were applied to remove details less than 0.25° thus avoiding aliasing effects. Finally, we resampled HC3 in both latitude and longitude at a step of 0.25° for the geographical coverage [-60°, 60°] in latitude and [-60°, 60°] in longitude. The resampled HC1 data set was adjusted by the *QMK* method onto the resampled HC3 data set for the common period of the 23 months. The adjustment was then applied to the period January 1985 to January 2004 included, to yield the first part of the new data set. The second part was made of the resampled HC3 data set, from February 2004 up to December 2016. The SSRD-H3E, therefore, contains daily mean of irradiance in W m^{-2} contrary to the daily irradiation of HC1 and HC3.

The data are stored under the format HDF in a single file. Daily mean of irradiance at the top-of-the-atmosphere were calculated with the SG2 algorithm (Blanc, Wald, 2012) and are included in the data set. A DOI has been allotted to the new data set: www.doi.org/10.23646/385c3cd1-968e-4924-8c5c-17a098736aa6. Access to the data obeys the principles of data sharing in the Global Earth Observation System of Systems (GEOSS), and like HC1 (Lefèvre et al., 2014), the SSRD-H3E data set is part of the GEOSS Data Collection of Open Resources for

Everyone (GEOSS Data-CORE), which is a distributed pool of documented data sets with full, open and unrestricted access at no more than the cost of reproduction and distribution.

6.2 Validation of the SSRD-H3E data set

Two validations were performed by comparing the data G_{h3e} against the same WRDC measurements G_{wrdc} as before (Figs 1-3). In the first validation, all valid years were merged to yield the period 1985-2016, and in the second one, the comparison was performed for each single year. Table 3 reports the bias, standard deviation of errors, correlation coefficient and slope of the fitting line for the whole period 1985-2016 at each station. Values are given as irradiation or irradiance for the sake of comparison with the previous sections and other published works. Relative values in percent were computed by dividing the indicator by the mean daily irradiation.

Table 3. Accuracy of SSRD-H3E at each station, for the period 1985-2016

Station	Mean daily irradiation (J cm^{-2})	Bias			Standard deviation of errors			Correlation coefficient	Slope (unitless)
		(J cm^{-2})	(W m^{-2})	%	(J cm^{-2})	(W m^{-2})	%		
Toravere	1244	50	6	4	229	27	18	0.957	0.997
Valentia	1075	85	10	8	228	26	21	0.954	1.046
Wien	1234	-3	0	-0	219	25	18	0.964	0.991
Auxerre	1203	30	3	2	191	22	16	0.973	1.036
Payerne	1249	71	8	6	220	25	18	0.966	0.976
Carpentras	1542	78	9	5	179	21	12	0.978	0.973
Nice	1545	97	11	6	209	24	14	0.968	0.964
El Arish	1937	-42	-5	-2	158	18	8	0.972	0.967
Maputo	1897	-35	-4	-2	229	27	12	0.941	0.911

The bias ranges from -42 to 97 J cm^{-2} (-5 to 11 W m^{-2}). It is low at Toravere, Wien, Auxerre, El Arish, and Maputo. It is noticeable at Valentia, Payerne, Carpentras, and Nice. The standard deviation of errors is fairly constant, around 209-229 J cm^{-2} (24-27 W m^{-2}) with lows at 158, 179 and 191 J cm^{-2} (18, 21, and 22 W m^{-2}). The correlation coefficient is large and greater than 0.94. The slopes are very close to 1, with a low at Maputo.

Actually these indicators vary in time. The bias (Fig. 8), and its relative value (Fig. 9), offer variations in time that depend on the station. The relative values were computed by dividing the bias for a given year by the corresponding yearly mean of the daily irradiation. In the first years before 1989, the bias is positive (overestimation) at all stations except El Arish and Maputo where it is negative. There is a clear trend at all stations for the bias to converge towards 0 as time progresses. After 2004, this is clearly explained by the fact that SSRD-H3E is made from HC3 only, which is more accurate than HC1-QMK.

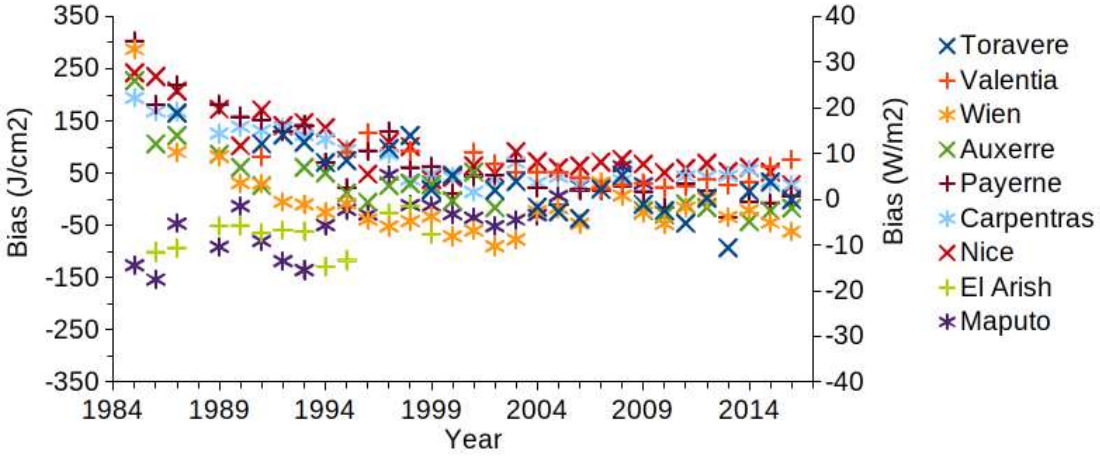

Figure 8. Bias in daily irradiation of the new data set SSRD-H3E for each year at each station in the period 1985-2016. In irradiance on right axis.

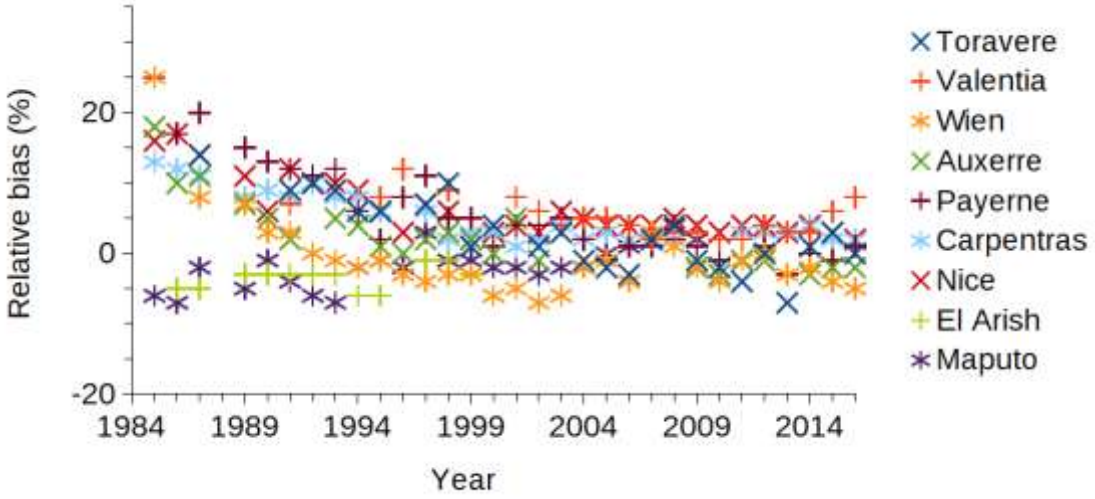

Figure 9. Bias in daily irradiation of the new data set SSRD-H3E for each year at each station relative to the yearly mean of the daily irradiation in the period 1985-2016

Variations in time may also be observed for the standard deviation of errors (Fig. 10), and its relative value (Fig. 11), and depend on the stations. El Arish exhibits small variation from 1985 to 2007 (no data available after), around 140 J m^{-2} (approx. 16 W m^{-2}). On the contrary, the other stations show two regimes: one before 2004 and one after. The period before 2004 is under the influence of HC1 even corrected by the fusion and there is more variability in the standard deviation than for the following period, which originates from HC3. Before 2004, the standard deviation is less than 250 J cm^{-2} (approx. 29 W m^{-2}) in most cases at all stations. After 2004, the standard deviation is less than 140 J cm^{-2} (approx. 16 W m^{-2}) in most cases at all stations and the variability is less for a given station. These two regimes appear clearly in relative values in Fig. 11.

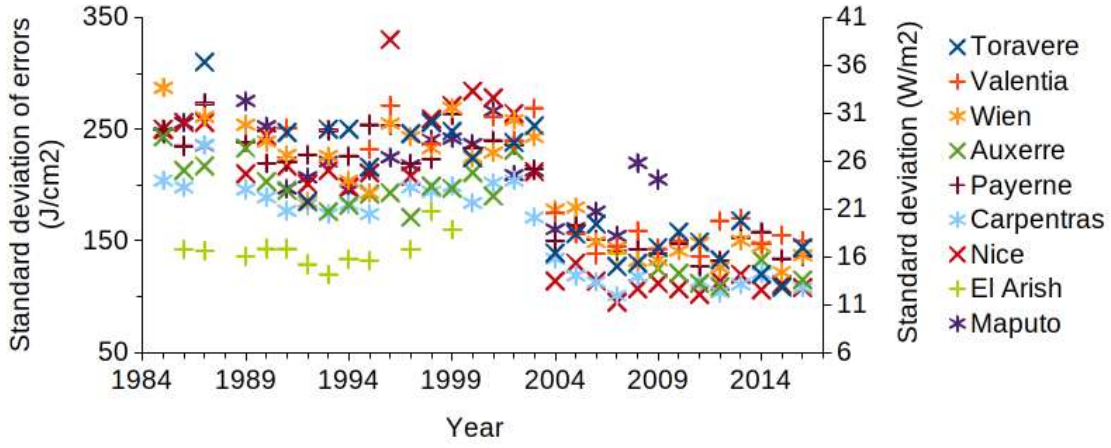

Figure 10. Standard deviation of errors in daily irradiation of the new data set SSRD-H3E for each year at each station in the period 1985-2016. In irradiance on right axis.

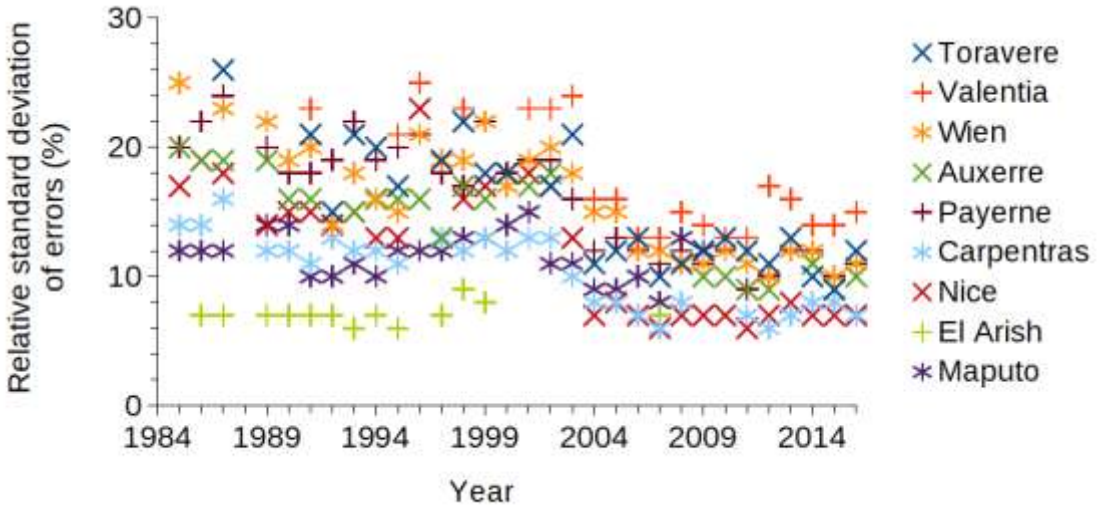

Figure 11. Standard deviation of errors in daily irradiation of the new data set SSRD-H3E for each year at each station relative to the yearly mean of the daily irradiation in the period 1985-2016

The correlation coefficient (Fig. 12) is large in all cases. The two regimes, before 2004 and after, are clearly visible. The correlation coefficients are highly variable before 2004. After 2004 they are greater than before and tend to approach unity. They are greater than 0.98 as a whole. Maputo is an exception with coefficients ranging from 0.94 to 0.97 for this period.

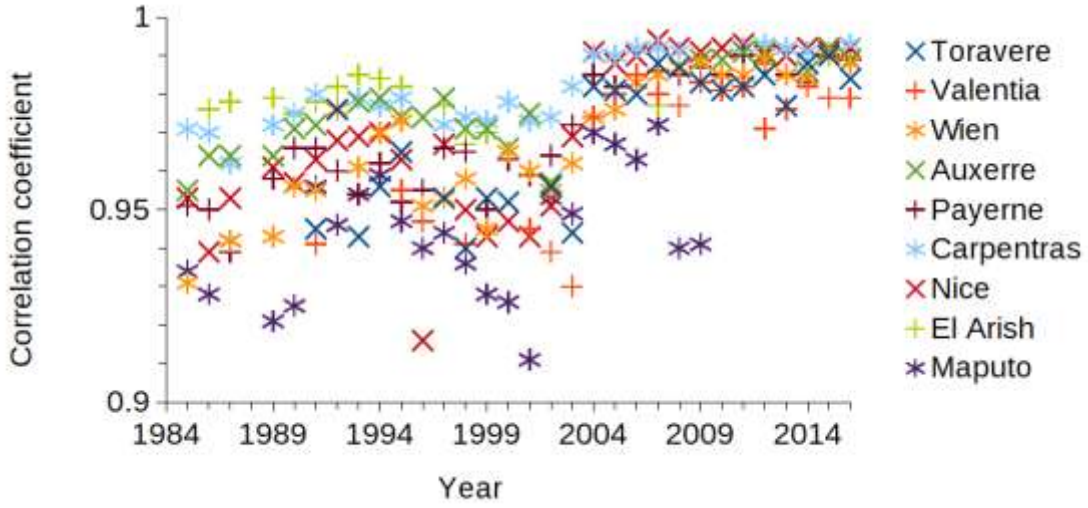

Figure 12. Correlation coefficient between WRDC measurements and SSRD-H3E estimates for each year at each station in the period 1985-2016

A similar behavior can be observed for the slopes of the fitting lines (Fig. 13). Prior to 2004, a large variability may be observed in slopes from year to year and from station to station, though the range of variation of the slopes is limited between 0.9 and 1.1, except for Maputo where the slopes are less than 0.9 for this period. After 2004, the slopes are closer to 1 at all stations and the variability is less: the range of variation is limited between 0.96 and 1.04.

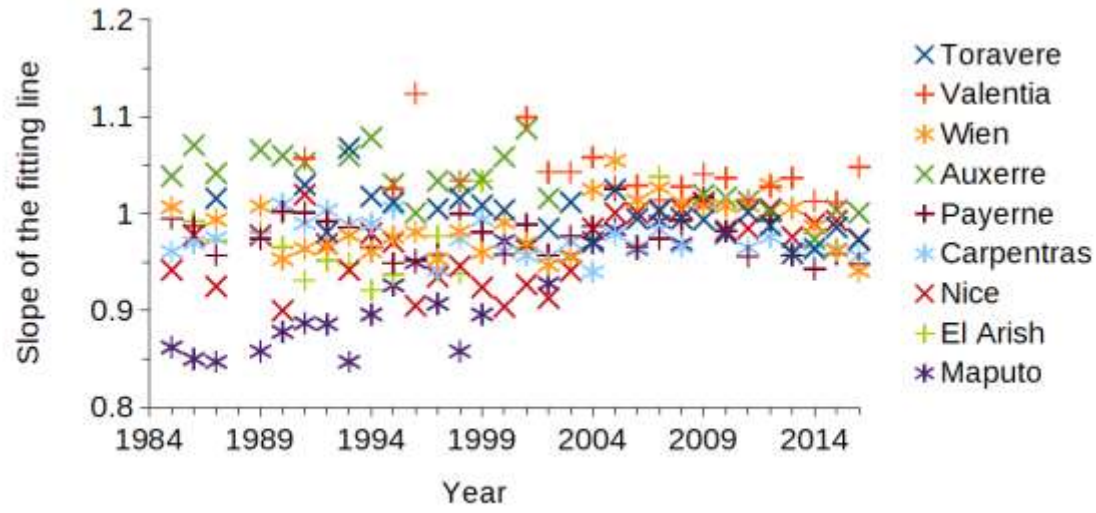

Figure 13. Slope of the fitting line between WRDC measurements and SSRD-H3E estimates for each period at each station in the period 1985-2016

A further visual inspection is made by drawing the mean of both G_{h3e} (in blue) and G_{wrdc} (in red) for each month of 1985-2016 in the same graph. Also drawn are the standard deviation of G_{h3e} (dashed line in light blue) and G_{wrdc} (dashed line in magenta) during each month. Expectations are that both the full lines on the one hand, and both the dashed lines on the other are superimposed. For the sake of space, only two stations, randomly selected, are presented: Wien (Fig. 14) and Maputo (Fig. 15). One may see that the monthly means are well reproduced by

SSRD-H3E. There are a few noticeable exceptions, such as an overestimation at Wien in July 1985, June 1986, or May 1989, and an underestimation in June-July 2016, or a slight underestimation in the first years at Maputo. The monthly standard deviations are also well reproduced by SSRD-H3E.

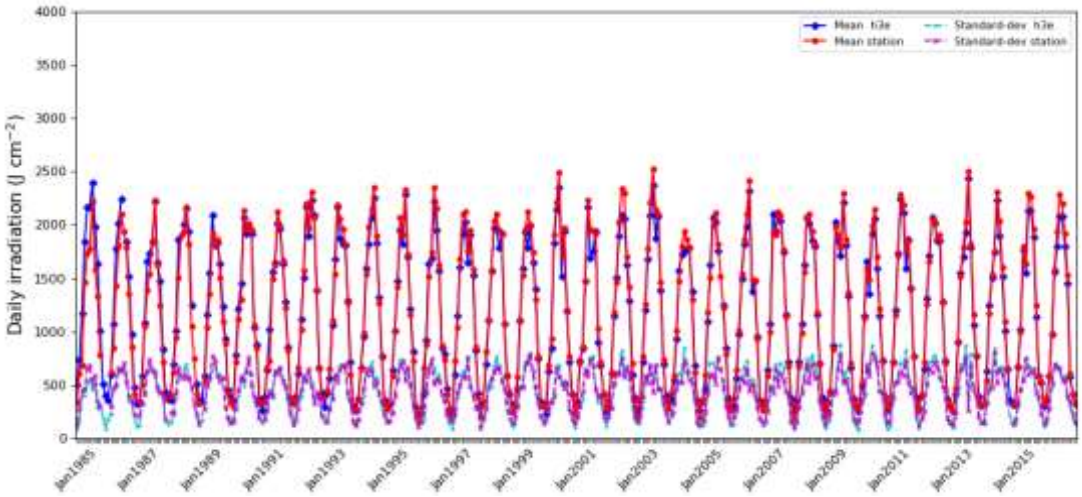

Figure 14. Monthly means and standard deviations from the WRDC data and SSRD-H3E estimates at Wien Hohe Warte in the period 1985-2016

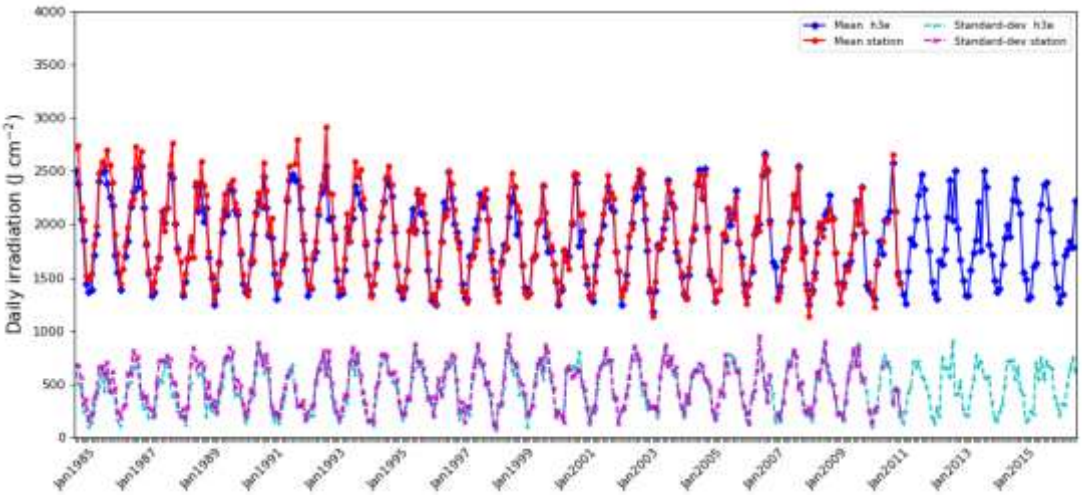

Figure 15. Monthly means and standard deviations from the WRDC data and SSRD-H3E estimates at Maputo in the period 1985-2016

7. Conclusions

This technical note has evaluated several methods aiming at improving the accuracy of the HC1 data set by fusion with the more accurate HC3 data set using an overlapping period of 23 months. The eight fusion methods tested here were fairly simple to implement with limited programming skills in Python, R or Matlab, or any language handling calls to web services, possibly in an automated way if building on the existing web services offering access to time series of the HC data sets.

The results of the several cases studied here shed light on the merits and drawbacks of each method and provided some guidance to users of the HC data sets so that they can implement themselves a fusion method. It was found that the simplest methods: *P50I*, *P50K*, *RatioI* and *RatioK*, bring limited benefit. Even more, instead of improving HC1, they may degrade its performance. Fusing the clearness index usually brings better results than fusing the irradiation. The methods *AffK* (affine function) and *QMK* (quantile mapping) perform the best, though degradation may be observed for the bias at several occasions. There are status quo or clear improvements of the standard deviation, correlation coefficient and slope of the fitting lines. As a whole, the authors note that the benefit brought by the two best methods is not always spectacular at all stations.

More sophisticated fusion methods may result in better performance. A simple example is the possible combination of the *QMK* and *P50K* methods in a cascade-type approach to avoid bias degradation. The task for an efficient fusion is complicated by the limited overlap of 23 months only between HC1 and HC3. If the fusion method calls upon statistical quantities, such as means, medians, cumulative distribution functions, which is the case of the eight methods here but *AffI* and *AffK* –and not on coincident time series of values like for *AffI* and *AffK*,- this limitation can be removed by using the whole data sets HC1 and HC3.

Other more complex mathematical tools may be used. One may also exploit the recent findings by Bengulescu et al. (2018) who reported that any time series of daily irradiation is composed of several characteristic timescales of variability, some having a deterministic origin, such as the yearly cycle, and others being realizations of various stochastic processes. One may devise a fusion method that comprises several sub-methods that are dependent on the timescale and the stochastic nature of the timescale.

The new SSRD-H3E data set has been created by the concatenation of the HC1e data set resulting from the *QMK* method between 1985 and January 2004 (included) and the HC3 data set for the following days. It offers 1985-2016 time-series of daily irradiation over Europe and Africa with a spatial resolution of 0.25°. The data set has been conceived as a simple and tractable means for the verification of models and for the adjustment of reanalyses and climate-change projections as discussed in e.g. Babst et al. (2008) with a spatial resolution close to those of the reanalyses and climate-change projections to ease the comparison and adjustment. Comparison with measurements made at nine stations for 15 periods of 2 years shows that the bias is variable with time for the early years. The standard deviation of errors is the greatest for the early years but is less than 250 J cm^{-2} (approx. 29 W m^{-2} for daily mean of irradiance). After 2004 (included), the standard deviation is less than 140 J cm^{-2} (approx. 16 W m^{-2}). The correlation coefficient is always large and always greater than 0.92.

No direct comparison was made against reanalyses or other similar products. However, it can be speculated that the SSRD-H3E data set compares favorably to the reanalyses, given published results of comparisons between such reanalyses and measurements performed at terrestrial or marine stations. For similar stations, Boilley and Wald (2015) have reported standard deviations of errors, and correlation coefficients for the MERRA and ERA-Interim re-analyses and HC1. They found superior performances for HC1. For reanalyses, though there is not enough information to perform its detailed calculations, the standard deviation of errors is typically 350 J cm^{-2} (approx. 41 W m^{-2}) as a whole; the reported correlation coefficients may be much less than 0.8. Trolliet et al. (2018) published a comparison of measurements performed within the PIRATA network in the tropical Atlantic Ocean against several satellite-derived data sets, including HC3, and the ERA5 and MERRA-2 reanalyses. They found superior performances for the satellite-derived data sets. The standard deviation of errors is typically 320 J cm^{-2} (approx. 47 W m^{-2}) for ERA5 and 420 J cm^{-2} (approx. 49 W m^{-2}) for MERRA-2 whereas it is190 J cm^{-2}, approx. 22 W m^{-2} for HC3. The reported correlation coefficients may be much less than 0.6 for ERA5 and 0.5 for MERRA-2 and is always greater than 0.87 for HC3. Of course, reanalyses have their merits, including other meteorological variables, worldwide geographical coverage and several decades back in time. The irradiation of a reanalysis may be corrected by the means of the SSRD-H3E, possibly using one the presented methods, though care must be taken when adjusting only one variable in a set of consistent and not independent meteorological variables (Dekens et al., 2017).

Other sources of SSRD over the Meteosat coverage or broader are available. Among them are the data sets established by the Satellite Application Facility on Climate Monitoring (CM-SAF) of Eumetsat. The CLARA-A2 data record covers the period 1982 until 2015 and is derived from the AVHRR (Advanced Very High Resolution Radiometer) sensor carried by polar-orbiting, operational meteorological satellites (Karlsson et al.,

2017). It offers daily means of irradiance with a spatial resolution of 0.25°. As written above, the SARAH-2 data set is derived from Meteosat images (Pfeifroth et al., 2017). It offers 30 min values of SSRD with a spatial resolution of 0.05° for the period starting in 1983. A slightly different version is also proposed, called SARAH-JRC (Urraca et al., 2017). Also available are HC3v5 of course and the Copernicus Atmosphere Monitoring Service (CAMS) Radiation Service (Qu et al., 2017), abbreviated as CRS. These two latter data sets begin in 2004 and offer 15 min SSRD with the same resolution than the SEVIRI pixels, i.e. 3 km at nadir and degrading as the satellite viewing angle is increasing. Several works have compared the quality of HC3v5 and CRS and have reported a slightly better quality for HC3v5, see Trolliet et al. (2018) and its references. Trolliet et al. (2018) also performed a comparison between SARAH-2, CRS and HC3v5 for daily means of irradiance in the tropical Atlantic Ocean for the period 2012-2013 and reported fairly similar performances between the three data sets. It can thus be speculated that at the spatial resolution of 0.25°, the SSRD-H3E data set offers the same quality than the SARAH-2 data set for the period starting in 2004, and surpasses the CRS data set. One may not conclude for the previous periods but one may note that Pfeifroth et al. (2018) reported better performances of SARAH-2 in the period 1992-2015 than in the period 1983-1991 in agreement with our findings for SSRD-H3E (graphs 8 to 13).

Urraca et al. (2017) have assessed the quality level of the daily means of the SARAH-JRC and CLARA-A2 data sets against ground measurements in Europe for 2005 to 2015. Though comparison between their results and ours in Table 3 is difficult because of the differences in period, in stations and in spatial resolution for SARAH-JRC, one may note that performances are fairly similar between these products and SSRD-H3E for the bias taking into account that all products exhibit large changes from station to station. Table 3 in Urraca et al. (2017) reports the average of the biases and the standard deviation. If one assumes a normal law for the statistical distribution of the bias, 95 % of the bias are in the range [-8, 9] W m^{-2} for SARAH-JRC and [-7, 9] W m^{-2} for CLARA-A2, which are close to the range [0, 11] W m^{-2} reported in our own Table 3 for the European stations. A more thorough analysis is necessary to draw solid conclusions.

Acknowledgments: The authors thank all ground station operators of the WMO network for their valuable measurements. They additionally thank the World Radiation Data Centre for hosting a website for downloading data. The authors thank the French company Transvalor, which takes care of the SoDa Service for the common good, thus providing an efficient access to the HelioClim databases. They are grateful to Philippe Blanc who designed the spatial low-pass filter used in the construction of the SSRD-H3E data set.

Appendix A – Python code for adjustment based on quantile mapping

This annex provides a pseudo code in Python for implementing an adjustment based on quantile mapping.

```
import numpy as np

# Use the function matching_histogram_t described hereafter to compute the empirical cumulative distribution functions of Ghc1 and Ghc3, or KThc1 and KThc3, for the period 2004-2005, then the transfer function funcI or funcK of the empirical cumulative distribution function of Ghc1 or KThc1 into that of Ghc3 or KThc3, and eventually apply this transfer function to Ghc1 or KThc1 for 1985-2005.

# Invalid values in time series are noted as np.NAN (not a number)

# Adjustment of irradiation G to yield G_hcQMI
    maxValue = np.max(G0_1985-2005)
    funcI = matching_histogram_t(Ghc3_2004-2005, Ghc1_2004-2005, maxValue)
    irradQmI = funcI(Ghc1_1985-2005)
```

```
# Adjustment of clearness index KT
    funcK = matching_histogram_t(KThc3_2004-2005, KThc1_2004-2005, 1.0)
    ktQmK = funcK(KThc1_1985-2005)

class matching_histogram_t:
    def __init__(self, x, y, maxValues):
        # adjust the values of a series y so that its histogram match that of the series x
        # x and y have the same length
        # return the adjusted y

        x = np.array(x, copy=True)
        y = np.array(y, copy=True)

        mask = np.isfinite(x)&np.isfinite(y)
        if np.all(~mask):
            yr1 = np.array([0.0, 1.0], dtype='f8')
            ya1 = np.array([np.NAN, np.NAN], dtype='f8')
            self.yr = np.linspace(0.0, maxValues, 100)
            self.ya = np.interp(self.yr, yr1, ya1)
            return

        x = x[mask]
        y = y[mask]

        # get the set of unique values and their corresponding indices and counts for x and y
        x_values, x_val_index = np.unique(x, return_inverse=True)
        x_freq = np.bincount(x_val_index)
        y_values, y_val_index = np.unique(y, return_inverse=True)
        y_freq = np.bincount(y_val_index)

        # take the cumsum of the frequencies, normalize by the number of values and get the empirical cumulative distribution functions
        x_quantiles = np.cumsum(x_freq).astype(np.float64)
        x_quantiles /= x_quantiles[-1]
        y_quantiles = np.cumsum(y_freq).astype(np.float64)
        y_quantiles /= y_quantiles[-1]

        # interpolate linearly to find the values in the x series that correspond most closely to the quantiles in the y series
        interp_x_values = np.interp(y_quantiles, x_quantiles, x_values)
        y_adjusted = interp_x_values[y_val_index]
        y_adjusted = np.clip(y_adjusted, 0.0, maxValues)

        # create f_adjust function that map y to y_adjusted.
        y_argsort = np.argsort(y)
        yr0 = y[y_argsort]          # < store unadjusted y
        ya0 = y_adjusted[y_argsort]         # < store adjusted y corresponding to yr0

        # remove invalid values
        mask = np.isfinite(yr0)&np.isfinite(ya0)
        yr0 = yr0[mask]
        ya0 = ya0[mask]
```

```
        # add bound values, (0.0, 0.0) and (1.0, 1.0)
        yr1 = np.empty((yr0.shape[0]+2,))       # < yr0 with bound
        ya1 = np.empty((ya0.shape[0]+2,))       # < ya0 with bound

        yr1[1:-1] = yr0
        ya1[1:-1] = ya0

        # set minimum and maximum bounds
        yr1[0] = 0.0
        ya1[0] = 0.0
        yr1[-1] = maxValues
        ya1[-1] = maxValues

        del yr0     # save few memory
        del ya0     # save few memory

        # resample (yr1, ya1) to the final (yr, ya) that have 100 points and make the f_adjust smoother.
        self.yr = np.linspace(0.0, maxValues, 100)
        self.ya = np.interp(self.yr, yr1, ya1)

        del yr1     # save few memory
        del ya1     # save few memory

    def __call__(self, y_to_adjust):
        return np.interp(y_to_adjust, self.yr, self.ya)
```

References

Amillo, A. G.; Huld, T.; Müller, R. A new database of global and direct solar radiation using the Eastern Meteosat Satellite, models and validation. Remote Sens. 2014, 6, 8165-8189, doi: 10.3390/rs6098165.

Babst, F.; Mueller, R. W.; Hollmann, R. Verification of NCEP reanalysis shortwave radiation with mesoscale remote sensing data. IEEE *Geosci. Remote Sens. Lett.* 2008, 5, 34-37, doi: 10.1109/LGRS.2007.907537.

Bengulescu, M.; Blanc, P.; Wald, L. On the intrinsic time-scales of temporal variability in measurements of the surface solar radiation. *Nonlinear Process. Geophys.* 2018, 25, 19-37, doi: 10.5194/npg-25-19-2018.

Blanc, P.; Gschwind, B.; Lefèvre, M.; Wald, L. The HelioClim project: Surface solar irradiance data for climate applications. Remote Sens. 2011, 3, 343-361, doi:10.3390/rs3020343.

Blanc, P.; Wald L. The SG2 algorithm for a fast and accurate computation of the position of the Sun. *Sol. Energy* 2012, 86, 3072-3083, doi: 10.1016/j.solener.2012.07.018.

Boilley, A.; Wald L. Comparison between meteorological re-analyses from ERA-Interim and MERRA and measurements of daily solar irradiation at surface. *Renew. Energ.* **2015**, 75, 135-143, doi: 10.1016/j.renene.2014.09.042.

Chen, M.; Zhuang, Q.; He, Y. An efficient method of estimating downward solar radiation based on the MODIS observations for the use of land surface modeling. *Remote Sens.* 2014, 6, 7136-7157, doi:10.3390/rs6087136.

Cros, S.; Albuisson, M.; Wald, L. Simulating Meteosat-7 broadband radiances at high temporal resolution using two visible channels of Meteosat-8. *Sol. Energy* 2006, 80, 361-367, doi: 10.1016/j.solener.2005.01.012.

Dekens, L.; Parey, S.; Grandjacques, M.; Dacunha-Castelle, D. Multivariate distribution correction of climate model outputs: A generalization of quantile mapping approaches: Multivariate distribution correction of climate model outputs. *Environmetrics* 2017, 28, doi: e2454. 10.1002/env.2454.

England, C.F.; Hunt, G.E. A study of the errors due to temporal sampling of the earth's radiation budget. Tellus 1984, 36B, 303-316.

Gschwind, B.; Ménard, L.; Albuisson, M.; Wald, L. Converting a successful research project into a sustainable service: the case of the SoDa Web service. *Environ. Modell. Softw.* 2006, 21, 1555-1561, doi:10.1016/j.envsoft.2006.05.002.

Hakuba, M. Z.; Folini, D.; Sanchez-Lorenzo, A.; Wild, M. Spatial representativeness of ground-based solar radiation measurements. *J. Geophys. Res. Atmos.* 2013, 118, 8585–8597, doi:10.1002/jgrd.50673.

Karlsson, K.-G.; Anttila, K.; Trentmann, J.; Stengel, M.; Meirink, J. F.; Devasthale, A.; Hanschmann, T.; Kothe, S.; Jääskeläinen, E.; Sedlar, J.; Benas, N.; van Zadelhoff, G.-J.; Schlundt, C.; Stein, D.; Finkensieper, S.; Håkansson, N.; Hollmann, R. CLARA-A2: the second edition of the CM SAF cloud and radiation data record from 34 years of global AVHRR data. *Atmos. Chem. Phys.* 2017, 17, 5809–5828, doi: 10.5194/acp-17-5809-2017.

Lefèvre, M.; Blanc, P.; Espinar, B.; Gschwind, B.; Ménard, L.; Ranchin, T.; Wald, L.; Saboret, L.; Thomas, C.; Wey, E. The HelioClim-1 database of daily solar radiation at Earth surface: an example of the benefits of GEOSS Data-CORE. *IEEE J. Sel. Topics Appl. Earth Observ. in Remote Sens.* 2014, 7, 1745-1753, doi:10.1109/JSTARS.2013.2283791.

Lefèvre, M.; Diabaté, L.; Wald, L. Using reduced data sets ISCCP-B2 from the Meteosat satellites to assess surface solar irradiance. *Sol. Energy* 2007, 81, 240-253, doi: 10.1016/j.solener.2006.03.008.

Lefèvre, M.; Oumbe, A.; Blanc, P.; Espinar, B.; Gschwind, B.; Qu, Z.; Wald, L.; Schroedter-Homscheidt, M.; Hoyer-Klick, C.; Arola, A.; Benedetti, A.; Kaiser, J. W.; Morcrette, J.-J. McClear: a new model estimating downwelling solar radiation at ground level in clear-sky condition. *Atmos. Meas. Tech.* 2013, 6, 2403-2418, doi: 10.5194/amt-6-2403-2013.

Müller, R.; Pfeifroth, U.; Träger-Chatterjee, C.; Trentmann, J.; Cremer, R. Digging the METEOSAT treasure—3 decades of solar surface radiation. Remote Sens. 2015, 7, 8067-8101, doi: 10.3390/rs70608067.

Pau, L. F. Sensor data fusion. *Journal of Intelligent and Robotics Systems* 1988, 1, 103-116.

Peel, M. C.; Finlayson, B. L.; McMahon, T. A. Updated world map of the Köppen-Geiger climate classification. *Hydrol. Earth Syst. Sci.* 2007, 11, 1633-1644, doi: 10.5194/hess-11-1633-2007.

Pfeifroth, U.; Kothe, S.; Müller, R.; Trentmann, J.; Hollmann, R.; Fuchs, P.; Werscheck, M. Surface Radiation Data Set - Heliosat (SARAH) - Edition 2. Satellite Application Facility on Climate Monitoring. doi: 10.5676/EUM_SAF_CM/SARAH/V002, 2017.

Pfeifroth, U.; Sanchez-Lorenzo, A.; Manara, V.; Trentmann, J.; Hollmann, R. Trends and variability of surface solar radiation in Europe based on surface- and satellite-based data records. *J. Geophys. Res.-Atmos.* 2018, 123, 1735–1754, doi: 10.1002/2017JD027418.Pinker, R.T.; Laszlo, I. Effects of spatial sampling of satellite data on derived surface solar irradiance. *J. Atmos. Oceanic Technol.* 1991, 8, 96-107.

Polo, J.; Wilbert, S.; Ruiz-Arias, J.A.; Meyer, R.; Gueymard, C.; Súri, M.; Martín, L.; Mieslinger, T.; Blanc, P.; Grant, I.; Boland, J.; Ineichen, P.; Remund, J.; Escobar, R.; Troccoli, A.; Sengupta, M.; Nielsen, K.P.; Renne, D.; Geuder, N.; Cebecauer, T. Preliminary survey on site-adaptation techniques for satellite-derived and reanalysis solar radiation datasets. *Sol. Energy* 2016, 132, 25-37, doi:10.1016/j.solener.2016.03.001.

Qu, Z.; Gschwind, B.; Lefèvre, M.; Wald, L. Improving HelioClim-3 estimates of surface solar irradiance using the McClear clear-sky model and recent advances in atmosphere composition. *Atmos. Meas. Tech.* 2014, 7, 3927–3933, doi:10.5194/amt-73927-2014.

Qu, Z.; Oumbe, A.; Blanc, P.; Espinar, B.; Gesell, G.; Gschwind, B.; Klüser, L.; Lefèvre, M.; Saboret, L.; Schroedter-Homscheidt, M.; Wald, L. Fast radiative transfer parameterisation for assessing the surface solar irradiance: The Heliosat-4 method, Meteorol. Z. 2017, 26, 33-57, doi:10.1127/metz/2016/0781.

Schiffer, R.; Rossow, W.B. ISCCP global radiance data set: A new resource for climate research. *Bull. Amer. Meteorol. Soc.* 1985, 66, 1498-1503.

Trolliet, M.; Walawender, J.P.; Bourlès, B.; Boilley, A.; Trentmann, J.; Blanc, P.; Lefèvre, M.; Wald, L. Estimating downwelling solar irradiance at the surface of the tropical Atlantic Ocean: A comparison of PIRATA measurements against several re-analyses and satellite-derived data sets. *Ocean Sci.* 2018, 14, 1021-1056, doi: 10.5194/os-14-1021-2018.

Urraca, R.; Gracia-Amillo, A. M.; Koubli, E.; Huld, T.; Trentmann, J.; Riihelä, A.; Lindfors, A. V.; Palmer, D.; Gottschalg, R.; Antonanzas-Torres, F. Extensive validation of CM SAF surface radiation products over Europe. *Remote Sensing of Environment* 2017, 199, 171-186, doi: 10.1016/j.rse.2017.07.013.

Wald, L. Some terms of reference in data fusion. IEEE Trans. Geosci. Remote Sens. 1999, 37, 1190-1193, doi: 10.1109/36.763269.

WMO: Guide to meteorological instruments and methods of observation, WMO-No 8, 2008 edition updated in 2010, World Meteorological Organization, Geneva, Switzerland, 2012.

Zelenka, A.; Perez, R.; Seals, R.; Renne, D. Effective accuracy of satellite-derived hourly irradiances. *Theoretical and Applied Climatology* 1999, 62: 199–207.

Zhao, L., Lee, X.; Liu, S. Correcting surface solar radiation of two data assimilation systems against FLUXNET observations in North America. *J. Geophys. Res.-Atmos.* 2013, 118, 9552–9564, https://doi.org/10.1002/jgrd.50697.